JOURNAL OF SPACECRAFT AND ROCKETS
Vol. 37, No. 4, July–August 2000

Identifying Slowly Varying and Turbulent Wind Features for Flight Loads Analyses

C. E. Spiekermann,* B. H. Sako,† and A. M. Kabe‡
The Aerospace Corporation, Los Angeles, California 90009-2957

A methodology is developed to determine the spectral boundary between wind features that can be considered slowly varying and the more rapidly varying, or turbulent, features of measured wind profiles. Pairs of measured wind velocity vs altitude profiles from the Eastern and Western launch ranges of the United States were used to establish the vertical wavelengths, which could no longer be considered slowly varying over discrete time intervals. Analyses were performed for wind pairs that were 30, 60, 90, and 120 min apart. The wavelength boundary between slowly varying and turbulent wind features as a function of time interval is presented. The results of this work now make it possible to identify and extract the slowly varying and turbulent wind features at a particular launch site. Identifying slowly varying and turbulent wind features is important in that it permits a potential reduction in the predicted loads on launch vehicles using measured wind profiles taken just prior to launch.

Nomenclature

A	= first measurement of a wind pair
B	= second measurement of a wind pair
f	= wind vertical wave number, cycles/ft
$f_{\text{ave},\Delta T}$	= boundary wave number for average ΔT coherence
$f_{n,\Delta T}$	= boundary wave number for nth ΔT wind pair
$\hat{G}_{u_A u_A}$	= power spectral density of A wind u component, $\text{ft}^3\ \text{s}^{-2}\ \text{cycle}^{-1}$
$\hat{G}_{u_A u_B}$	= cross-spectral density wind u components, $\text{ft}^3\ \text{s}^{-2}\ \text{cycle}^{-1}$
$N_{\Delta T}$	= number of wind pairs with time interval ΔT
n	= nth wind pair, $n = 1, 2, \ldots, N_{\Delta T}$
u	= zonal (west, east) component of wind
v	= meridional (south, north) component of wind
$\hat{\Gamma}^2_{\text{ave},\Delta T}$	= average coherence square across all ΔT wind pairs
$\hat{\Gamma}^2_{n,\Delta T}$	= weighted u, v coherence square for nth ΔT wind pair
$\hat{\Gamma}^2_{u_A u_B}$	= coherence square for wind pair u components
ΔT	= time interval between wind measurements, min
λ	= atmospheric wind vertical wavelength, ft
$\lambda_{\text{ave},\Delta T}$	= wavelength corresponding to $f_{\text{ave},\Delta T}$, ft
$\lambda_{n,\Delta T}$	= boundary wavelength corresponding to $f_{n,\Delta T}$, ft
$\bar{\lambda}_{n,\Delta T}$	= mean boundary wavelength, all ΔT wind pairs, ft
$\sigma_{n,\Delta T}$	= standard deviation of boundary wavelengths, ft
$\wedge$	= estimated parameter

Introduction

AERODYNAMIC pressure acting on a launch vehicle during atmospheric flight is a significant source of structural loading.[1,2] This loading is greatly influenced by the atmospheric wind through which the vehicle flies.[3–6] Loads analyses are typically divided into those that can be performed just prior to launch and those that have to be completed prior to the day of launch.[7,8] Both sets of loads are then combined statistically just prior to launch to estimate the total vehicle loads that are then compared to the allowable values.[9–12]

A vertical wavelength can be thought of as an altitude-dependent wind feature, which modulates the angle of attack of a launch vehicle as it flies through the wind. There may be many spectral components of various vertical wavelengths present within any altitude sample of a wind profile. Spectral analysis is possible, where the independent variable is altitude. Loads calculations performed on the day of launch are reasonable for that portion of the load that is associated with the slowly varying vertical wavelengths in the wind velocity vs altitude profile. Typical wind profiles containing both the slowly varying and the turbulent features of the wind are shown in Figs. 1 and 2 for a pair of balloon measurements.

It is intuitive that longer vertical wavelengths are more slowly varying over time than shorter wavelengths. It is evident in Figs. 1 and 2 that the longer vertical wavelengths are more slowly varying and that the shorter vertical wavelengths vary much more over time. The variation is more evident as the time interval increases from 30 to 90 min in Figs. 1 and 2. Loads caused by the rapidly varying or turbulent components of the wind should be treated statistically and independent of the measured day-of-launch wind. To do this, it is critical that the boundary between the slowly and rapidly varying components of the wind be identified.

Procedure

The coherence-squared function applied to wind pairs form the basis here for determining the wave number f, which defines the spectral boundary between the slowly varying and the turbulent wind features. A wave number[13] represents the number of waves of a particular wavelength in a unit distance. A wave number is also the inverse of the wavelength λ, the distance between two successive crests of a single periodic component in the vertical wind profile. Denote (U_A, V_A) to be the zonal (u, west–east) and meridional (v, south–north) components of the A-wind measured at some given instance and (U_B, V_B) to be the B-wind, occurring ΔT minutes later. In day-of-launch operations the A-wind will be known from measurements, and the unknown B-wind is the wind profile through which the launch vehicle will fly. Therefore, the B-wind is viewed as a perturbation of the A-wind. In terms of the u component, we would have at any altitude h

$$U_B(h) = U_A(h) + N_U(h) \tag{1}$$

where N_U is the u-noise component accounting for nonpersistent changes in U_A. The coherence-square function for the u component of a pair of A and B winds is defined by

$$\Gamma^2_{U_A U_B}(f) = \frac{\left| G_{U_A U_B}(f) \right|^2}{G_{U_A U_A}(f) G_{U_B U_B}(f)} \tag{2}$$

where, $G_{U_A U_B}$, is the cross-spectral density (CSD) function of U_A and U_B and $G_{U_A U_A}$ and $G_{U_B U_B}$ are the power spectral density (PSD) functions of U_A and U_B, respectively.

Presented as Paper 99-1250 at the AIAA/ASME/ASCE/AHS/ASC 40th Structures, Structural Dynamics, and Materials Conference, St. Louis, MO, 12–15 April 1999; received 15 December 1999; revision received 14 April 2000; accepted for publication 18 April 2000.

*Engineering Specialist, Structural Dynamics Department, P.O. Box 92957-M4/909. Member AIAA.

†Senior Engineering Specialist, Structural Dynamics Department, P.O. Box 92957-M4/915. Member AIAA.

‡Director, Structural Dynamics Department, P.O. Box 92957-M4/911. Senior Member AIAA.

Table 1 Monthly distribution of wind pairs evaluated from both ER and WR that were measured 30, 60, 90, and 120 min (± 5 min) apart

	ER wind pairs					WR wind pairs					
Month	30	60	90	120	Sum	30	60	90	120	Sum	Total
January	0	3	29	24	56	10	12	14	20	56	112
February	12	17	42	42	113	4	6	14	11	35	148
March	13	11	22	28	74	2	7	9	16	34	108
April	8	14	25	26	73	20	19	7	17	63	136
May	4	6	21	17	48	4	5	14	20	43	91
June	3	4	10	11	28	0	2	11	7	20	48
July	1	6	22	23	52	0	4	9	10	23	75
August	5	8	31	18	62	0	1	13	8	22	84
September	0	4	37	17	58	2	2	15	7	26	84
October	1	9	20	14	44	8	13	7	6	34	78
November	4	8	22	16	50	0	4	13	15	32	82
December	1	10	23	17	51	9	10	8	10	37	88
Sum	52	100	304	253	709	59	85	134	147	425	1134

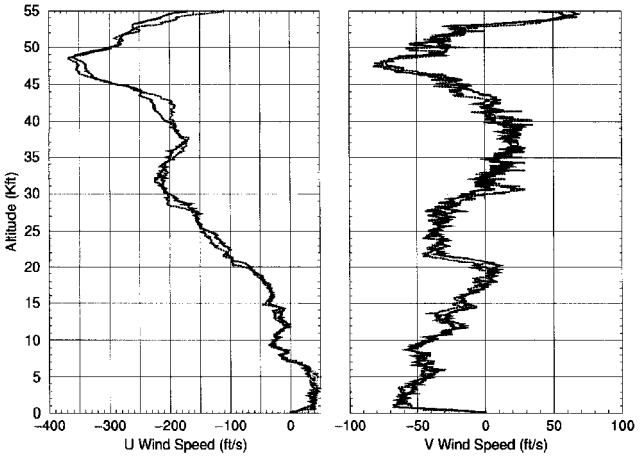

Fig. 1 Example profiles of a 30-min wind pair from ER measured 870318 at 1630 and 1700 z.

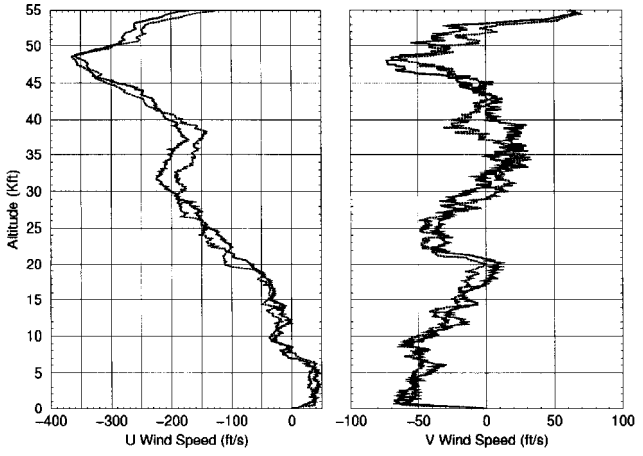

Fig. 2 Example profiles of a 90-min wind pair from ER measured 870318 at 1630 and 1800 z.

If we assume that N_U is uncorrelated to U_A, then Eq. (2) simplifies to

$$\Gamma^2_{U_A U_B}(f) = 1 \Big| \left[1 + G_{N_u N_u}(f) \Big| \; G_{U_A U_A}(f)\right] \tag{3}$$

which gives a coherence-squared value of 0.5 for a signal-to-noise ratio of 1. Because longer wavelength wind features are more slowly varying, we would expect $\Gamma^2_{U_A U_B}$ to be monotonically decreasing with wave number f. Therefore, the wave number for which the coherence-square value is equal to 0.5 will be used here to define the spectral boundary between the slowly varying and turbulent wind features.

Similarly, define the coherence-squared function for the v component of a pair of A and B winds by

$$\Gamma^2_{V_A V_B}(f) = \frac{\left| G_{V_A V_B}(f) \right|^2}{G_{V_A V_A}(f) G_{V_B V_B}(f)} \tag{4}$$

To determine a spectral boundary between slowly varying and turbulent wind features, which is applicable to both u and v components, the coherence-squared functions in Eqs. (2) and (4) can be combined using a PSD weighted average. Specifically, let

$$\theta_U(f) = \frac{G_{U_A U_A}(f) + G_{U_B U_B}(f)}{G_{U_A U_A}(f) + G_{U_B U_B}(f) + G_{V_A V_A}(f) + G_{V_B V_B}(f)} \tag{5}$$

$$\theta_V(f) = \frac{G_{V_A V_A}(f) + G_{V_B V_B}(f)}{G_{U_A U_A}(f) + G_{U_B U_B}(f) + G_{V_A V_A}(f) + G_{V_B V_B}(f)} \tag{6}$$

represent the fraction of the total energy for the u and v components, respectively. The weighted average coherence-squared function for a given wind pair is defined as

$$\Gamma^2_{\text{ave}} = \theta_U \cdot \Gamma^2_{U_A U_B} + \theta_V \cdot \Gamma^2_{V_A V_B} \tag{7}$$

The wave number f determined from

$$\Gamma^2_{\text{ave}}(f) = 0.5 \tag{8}$$

is taken to be the boundary, which spectrally separates the slowly varying and turbulent wind features.

Computation of the coherence-squared function is accomplished using the discrete Fourier transform (DFT) as described in Bendat and Piersol.[14] For each wind pair, only winds corresponding to altitudes between 5 and 50 kft were used. Estimation of the CSD and PSD, which appear in the numerator and denominator of Eqs. (2) and (4), was performed using a 50% overlapping process with a DF T block size corresponding to 10 kft. Additionally, each data block had its mean removed and was tapered using a Hanning window prior to applying the DFT.

Overview of Study

Measured wind profiles, consisting of wind speed and direction as a function of altitude in 100-ft increments from approximately the ground to approximately 50 kft, were gathered from an extensive historical winds database. These profiles are typically displayed as the zonal and the meridional wind magnitude components (Fig. 1). Only wind profiles measured with Jimsphere balloons were used because they are known to have better vertical resolution than Windsonde balloons, the other common measurement system.[15–18] Wind profiles with significant data gaps were excluded from this study.

The winds represented all months of the year dating back to 1964 at both the Eastern Range (ER) in Florida and the Western Range (WR) at Vandenberg Air Force Base in California (Tables 1 and 2). Wind pairs were identified where the time interval between

Table 2 Yearly distribution of wind pairs evaluated from both ER and WR that were measured 30, 60, 90, and 120 min (± 5 min) apart

	ER wind pairs					WR wind pairs					
Year	30	60	90	120	Sum	30	60	90	120	Sum	Total
1964	——	——	2	——	2	——	——	——	——	0	2
1965	——	5	5	3	13	——	——	10	——	10	23
1966	——	3	4	6	13	——	——	11	——	11	24
1967	——	7	29	21	57	——	1	5	1	7	64
1968	1	2	24	7	34	——	——	2	——	2	36
1969	——	——	10	3	13	——	——	——	——	0	13
1970	——	——	——	1	1	——	——	——	——	0	1
1971	——	——	6	——	6	——	4	——	3	7	13
1972	——	——	11	13	24	——	1	6	1	8	32
1973	——	——	22	——	22	——	——	——	——	0	22
1974	——	——	27	——	27	——	——	——	——	0	27
1975	——	——	11	——	11	——	——	——	——	0	11
1976	——	——	——	——	——	——	——	1	7	8	8
1977	——	——	5	44	49	——	——	——	39	39	88
1978	——	——	——	——	——	——	——	2	1	3	3
1979	——	——	——	——	——	——	1	——	——	1	1
1980	——	——	——	——	——	——	——	1	1	2	2
1984	——	——	——	——	——	——	——	1	——	1	1
1987	23	15	110	107	255	——	——	82	64	146	401
1988	——	——	18	13	31	——	——	13	16	29	60
1989	——	——	——	1	1	23	22	——	——	45	46
1990	——	6	——	4	10	36	37	——	——	73	83
1991	2	3	2	1	8	——	——	——	——	0	8
1994	3	11	3	7	24	——	——	——	——	0	24
1995	14	9	9	3	35	——	6	——	6	12	47
1996	9	13	6	4	32	——	4	——	4	8	40
1997	——	26	——	15	41	——	9	——	4	13	54
Sum	52	100	304	253	709	59	85	134	147	425	1134

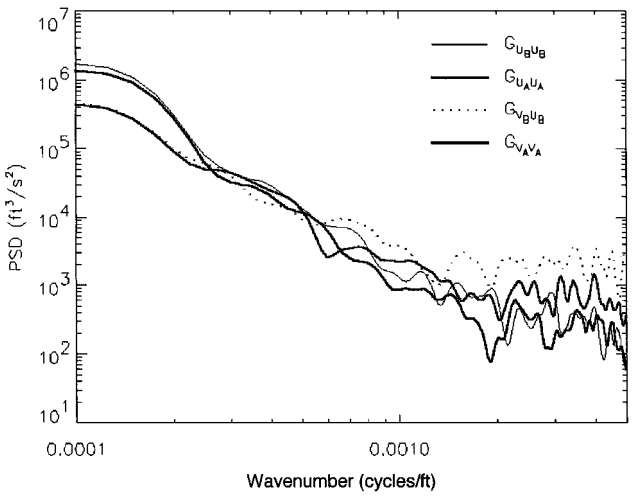

Fig. 3 Example power spectral density of a 30-min wind pair from ER measured 870318 at 1630 and 1700 z.

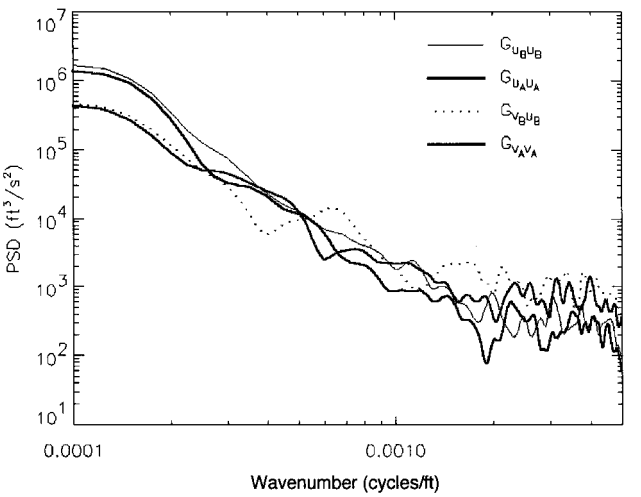

Fig. 4 Example power spectral density of a 90-min wind pair from ER measured 870318 at 1630 and 1800 z.

the measured wind profiles ΔT was 30, 60, 90, and 120 min (±5 min for each) (Table 1). These are the range of time intervals typically used during day-of-launch operations. There were 1134 wind pairs identified.

When initially looking at the wind profiles, it was obvious that the general trend was for vertical wavelengths to be less persistent as the time interval was increased. With a 30-min interval the two wind profiles typically appear somewhat similar (Fig. 1), but at larger time intervals it becomes obvious that the vertical wavelengths are less persistent (Fig. 2). This lack of persistence was then quantified in the following manner.

For each wind pair, PSD analyses were performed using the method described in the preceding section. The block size influences the smallest discernible wave number and the wave number resolution, whereas the wind profile altitude resolution determines the largest wave number because of the Nyquist constraint. Therefore, wave numbers between 0.0001 and 0.005 are displayed. These correspond to wavelengths between 10,000 and 200 ft. The PSDs were reviewed for reasonableness: the linearity typically observed in the measurable wave-number region and the start of the noise floor at roughly a 500-ft wavelength. Figures 3 and 4 are typical PSD plots of the wind profiles. The U and V wind components are approximately linear in the measurable range and reach the noise floor at a wave number of approximately 0.002 cycle/ft, or a wavelength of approximately 500 ft. There is little observable difference between the PSD plots of 30-min and 90-min wind pairs.

Next, coherence spectral analyses were performed on the u and the v wind components. Because these varied as a result of the differing energy in the u and v wind components, a single coherence spectrum was obtained by using the weighted average of the u and v wind components described earlier. For each coherence spectrum, the boundary wave number $f_{n,\Delta T}$ in cycle/ft, where the weighted coherence indicated that one wind in the pair could no longer be identified from the other, was established. The coherence boundary

for these wind pairs is easily identified by the weighted average coherence-squared function in Eq. (8) as

$$\hat{\Gamma}^2_{n,\Delta T}(f_{n,\Delta T}) \approx 0.5$$
$$n = 1, \ldots, N_{\Delta T}, \quad \Delta T = 30, 60, 90, 120 \quad (9)$$

Figures 5 and 6 show two examples. In Fig. 5, a 30-min wind pair, the weighted average wind components reach a coherence-square of 0.5 at 0.000348 cycle/ft, or 2872 ft/cycle. In Fig. 6, a 90-min wind pair, the weighted average wind components reach a coherence-square of 0.5 at 0.000202 cycle/ft, or 4950 ft/cycle.

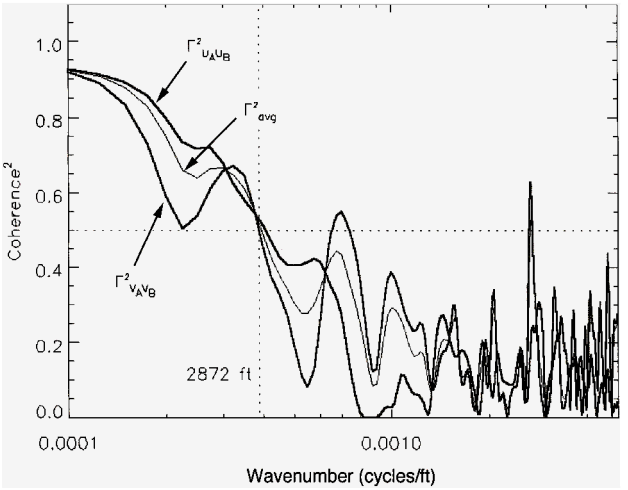

Fig. 5 Example of coherence squared of 30-min wind pair from ER measured 870318 at 1630 and 1700 z.

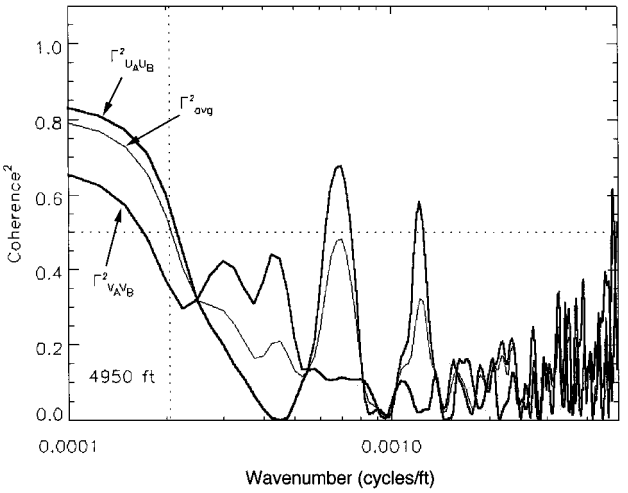

Fig. 6 Example of coherence squared of 90-min wind pair from ER measured 870318 at 1630 and 1800 z.

The selection of 0.5 for coherence square is not overly harsh because it does not require complete coherence, but simply identifies the wave number when the uncoherent portion of the wind pair becomes larger than the coherent portion. The corresponding boundary wavelength is equal to the inverse of the wave number, as shown in Eq. (10):

$$\lambda_{n,\Delta T} = 1/f_{n,\Delta T}, \quad n = 1, \ldots, N_{\Delta T}, \quad \Delta T = 30, 60, 90, 120 \quad (10)$$

A Wilcoxon rank sum test[19] was performed to test the hypothesis that the boundary wavelengths are statistically similar either between the ER and WR, or between the months containing winds that generally result in more severe launch-vehicle loads vs the other months of the year. The months with these more severe winds are defined here as the five months, December through April. It was determined that the ER and WR severe-month wind pairs coherence boundary wavelengths could be considered to be part of the same statistical family (Figs. 7–10). However, the more severe and the other months of the year should not be considered part of the same family, for either the ER or the WR. In Figs. 7–10 the parameter T represents the sum of the ranks of one of the data sets; Z is a standardized random variable using the mean and variance of T; and P is the probability that the standardized random variable of any other partial sum of the ranks z is less than Z. The probabilities P, shown in Figs. 7–10, indicate that the two data sets are statistically similar.

Therefore, a reasonably sized statistical sample was obtained by combining the ER and WR wind pairs from December through April. The number of wind pairs from the other months did not provide an adequate sample at all time intervals and are not addressed here. Only the severe-months wind pairs with a boundary wavelength shorter than 10,000 ft were considered during the remainder of the study. A total of 552 wind pairs was used (Table 3).

Results

The boundary wave numbers obtained from Eq. (9) are displayed in histograms in Figs. 11–14 for the 30-, 60-, 90-, and 120-min wind pairs. It is visually obvious that the mean and standard deviation of the wave numbers decreases as the wind-pair time interval increases. The specific values are presented in the figures. These distributions are not normal distributions. Each distribution has a positive skewness. The mean values are summarized in the left column of Table 4.

Similarly, an alternate view of the data is obtained from the boundary wavelengths from Eq. (10), which are displayed in histograms in Figs. 15–18. As expected, the mean and standard deviation of the wavelengths increases as the wind-pair time interval increases. These distributions also have a positive skewness. The wavelength means are summarized in the middle column of Table 4. The wave number and wavelength means for each of the time intervals would be expected to be different because the individual values are inversely related and have significant standard deviations; however, they are only approximately 15–20% different.

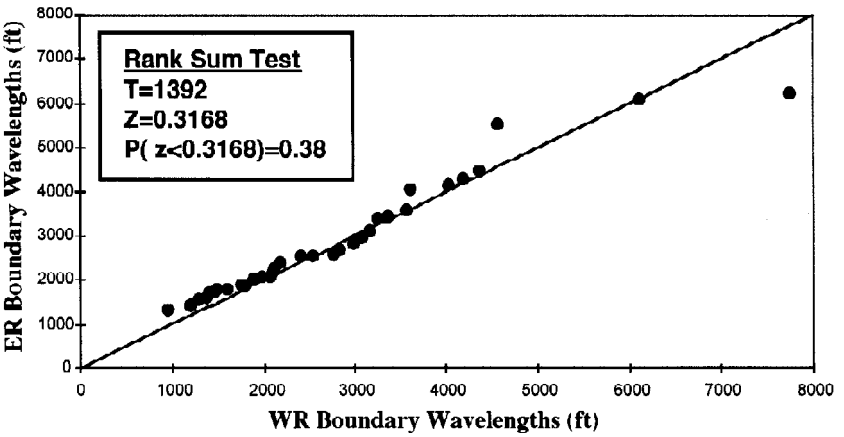

Fig. 7 Rank sum test for boundary wavelengths from 30-min pairs at ER and WR during December through April.

Table 3 Distribution of wind pairs evaluated from ER and WR

	ER wind pairs					WR wind pairs					
Month	30	60	90	120	Sum	30	60	90	120	Sum	Total
January	0	3	29	20	52	10	12	14	12	48	100
February	12	17	42	40	111	4	6	14	10	34	145
March	13	11	19	25	68	2	7	9	12	30	98
April	8	13	24	25	70	20	18	7	15	60	130
December	1	9	22	14	46	9	10	7	7	33	79
Sum	34	53	136	124	347	45	53	51	56	205	552

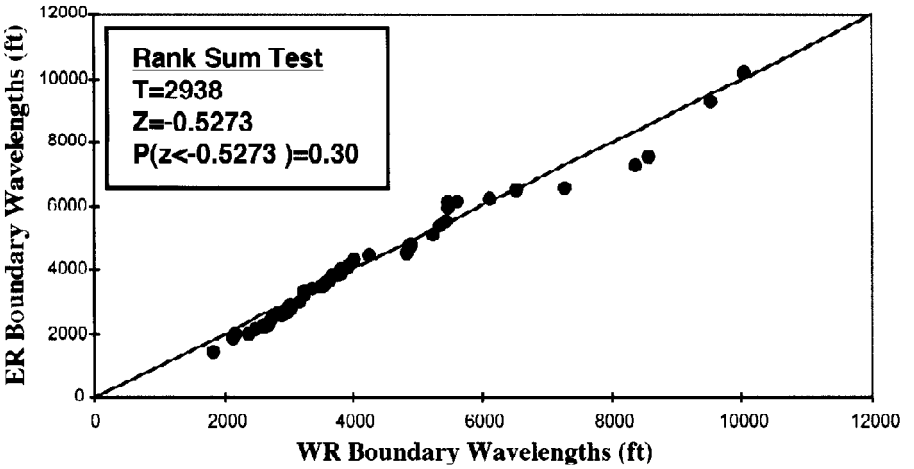

Fig. 8 Rank sum test for boundary wavelengths from 60-min pairs at ER and WR during December through April.

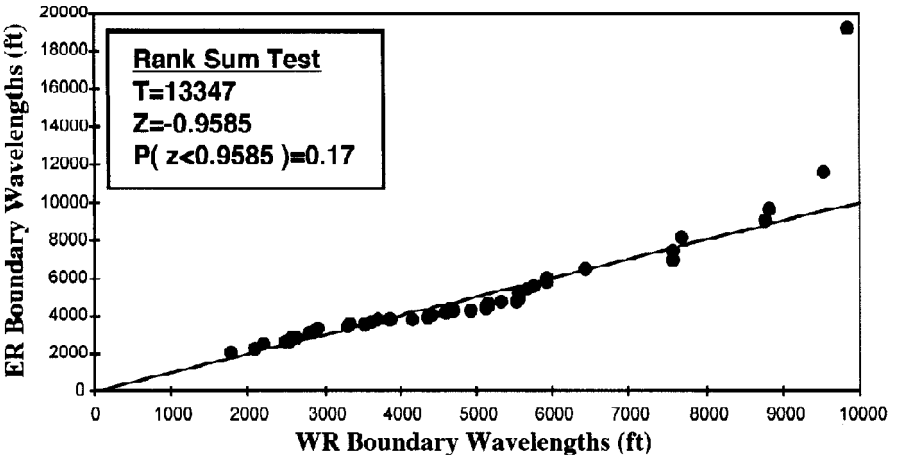

Fig. 9 Rank sum test for boundary wavelengths from 90-min pairs at ER and WR during December through April.

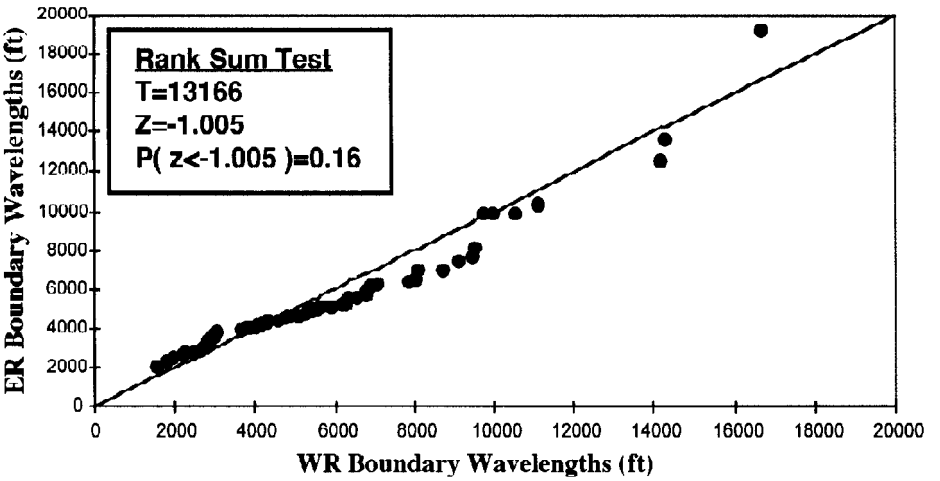

Fig. 10 Rank sum test for boundary wavelengths from 120-min pairs at ER and WR during December through April.

Table 4 Boundary wavelengths between slowly varying and turbulent atmospheric wind wavelengths

	Boundary wavelength, ft		
ΔT, min	From mean of wave numbers at coherence = 0.5	From mean of (1/wave numbers) at coherence = 0.5	From average coherence spectrum at coherence = 0.5
30	2304	2798	2528
60	3436	3965	3821
90	3952	4477	4346
120	4149	4725	4960

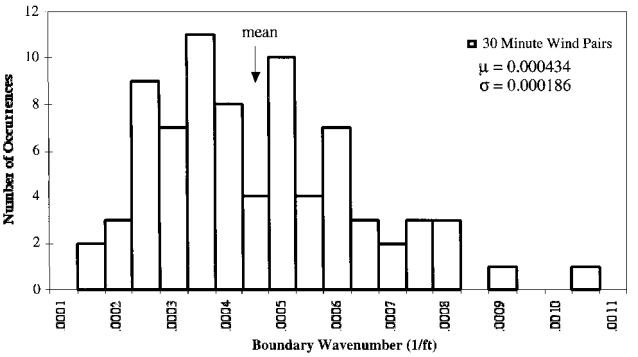

Fig. 11 Distribution of the 30-min wind pairs boundary wave numbers.

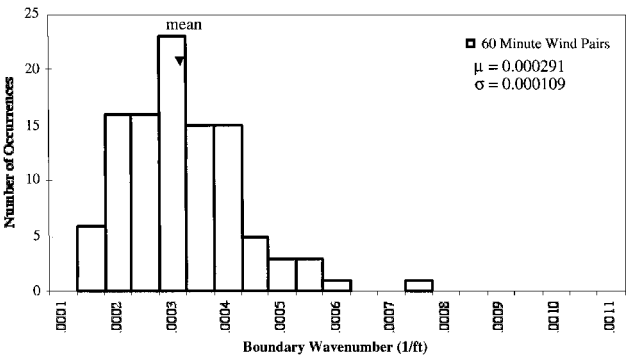

Fig. 12 Distribution of the 60-min wind pairs boundary wave numbers.

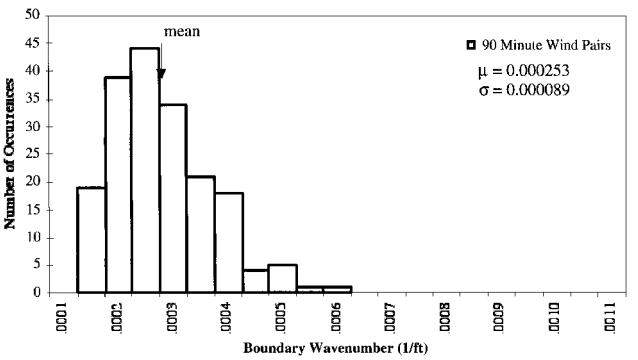

Fig. 13 Distribution of the 90-min wind pairs boundary wave numbers.

Another alternate view of the data was obtained by generating an average coherence spectrum from the individual coherence spectra for each time interval ΔT of 30, 60, 90, and 120 min:

$$\hat{\Gamma}^2_{\text{ave},\Delta T}(f) = \frac{1}{N_{\Delta T}} \sum_{n=1}^{N_{\Delta T}} \hat{\Gamma}^2_{n,\Delta T}(f), \qquad \Delta T = 30, 60, 90, 120 \quad (11)$$

From these, an average coherence boundary wave number was identified for each set of wind pairs (Figs. 19–22), i.e.,

$$\hat{\Gamma}^2_{\text{ave},\Delta T}(f_{\text{ave},\Delta T}) \approx 0.5, \qquad \Delta T = 30, 60, 90, 120 \quad (12)$$

$$\lambda_{\text{ave},\Delta T} = 1/f_{\text{ave},\Delta T}, \qquad \Delta T = 30, 60, 90, 120 \quad (13)$$

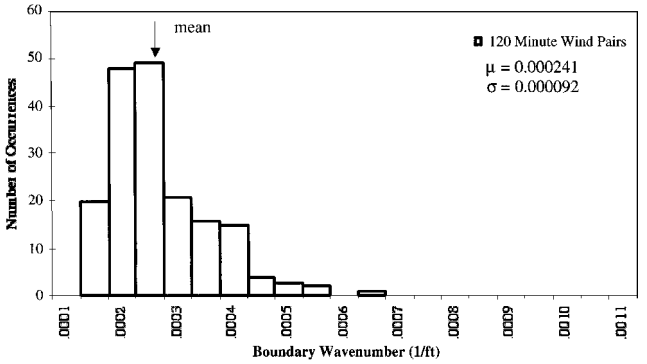

Fig. 14 Distribution of the 120-min wind pairs boundary wave numbers.

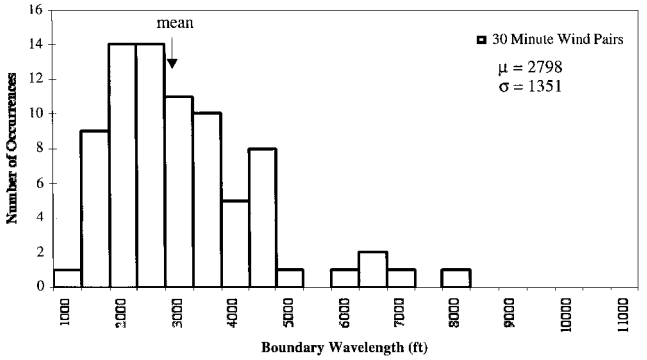

Fig. 15 Distribution of the 30-min wind pairs boundary wavelengths.

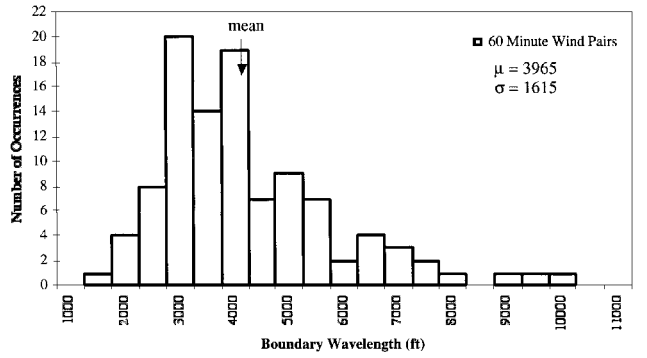

Fig. 16 Distribution of the 60-min wind pairs boundary wavelengths.

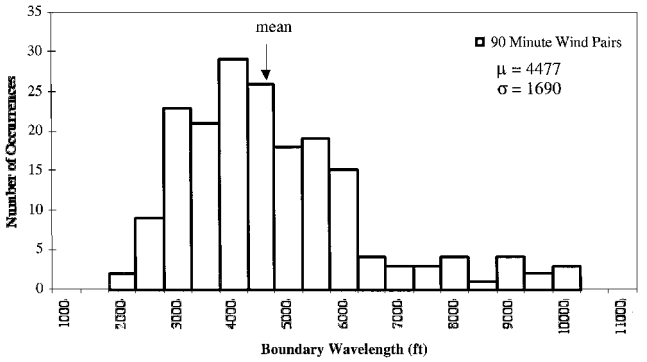

Fig. 17 Distribution of the 90-min wind pairs boundary wavelengths.

These are presented as wavelengths in the right-hand column of Table 4.

Wavelengths longer than those from Eq. (13) remain, on the average, slowly varying over the specified time interval. Wavelengths shorter than these values, on the average, should be considered non-persistent and hence represent turbulence. This averaging process again resulted in boundary wavelengths similar to the preceding statistical values in the first and second columns of Table 4. An advantage of this approach is that it is quantitative

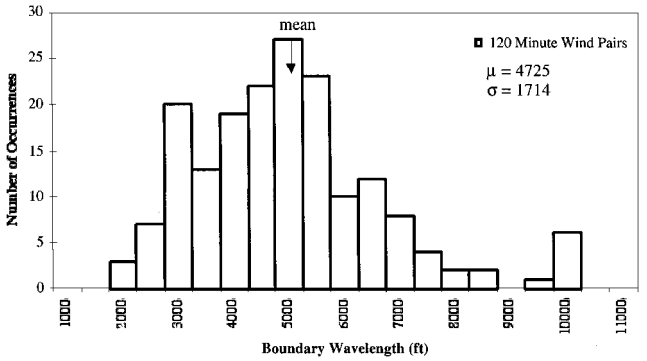

Fig. 18 Distribution of the 120-min wind pairs boundary wavelengths.

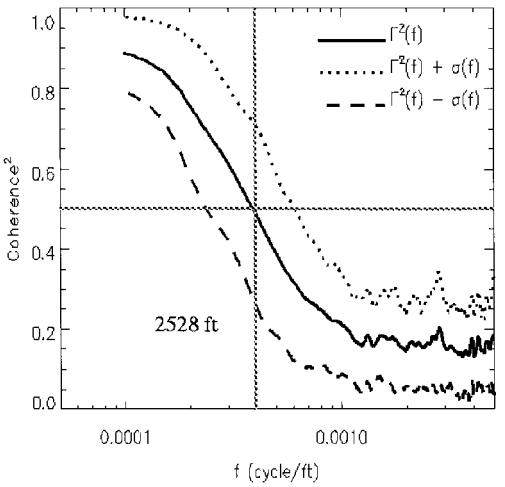

Fig. 19 Average coherence spectrum from 79 wind pairs measured 30 min apart.

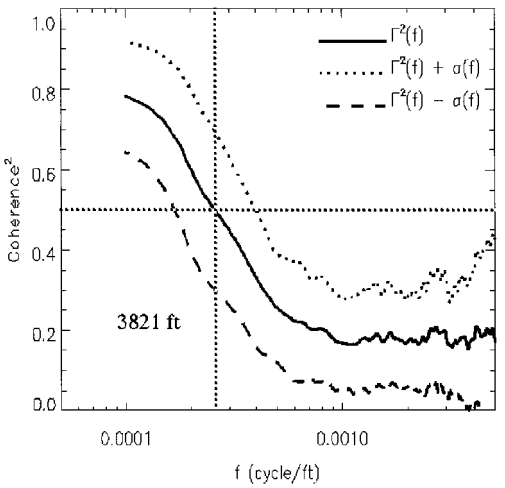

Fig. 20 Average coherence spectrum from 106 wind pairs measured 60 min apart.

and minimizes engineering judgment. Plots of Eqs. (12) and (13) are shown in Figs. 19–22. The 30-min wind pairs reach an average coherence-squareof 0.5 at a wavelengthof 2528 ft, the 60-min wind pairs at 3821 ft, the 90-min wind pairs at 4346 ft, and the 120-min wind pairs at 4960 ft. The plus and minus one standard deviation curves in Figs. 19–22 indicate the variation in the coherence squared and should not be used to establish the variance of the wavelengths.

Finally, a curve (Fig. 23) was fit through the four average coherence boundary wavelengths from the right column of Table 4 plus the origin because at $\Delta T = 0$ the wind pair should be coherent. An excellent fit of the data was found to be the following simple function:

$$\lambda_B = 460\sqrt{\Delta T} \tag{14}$$

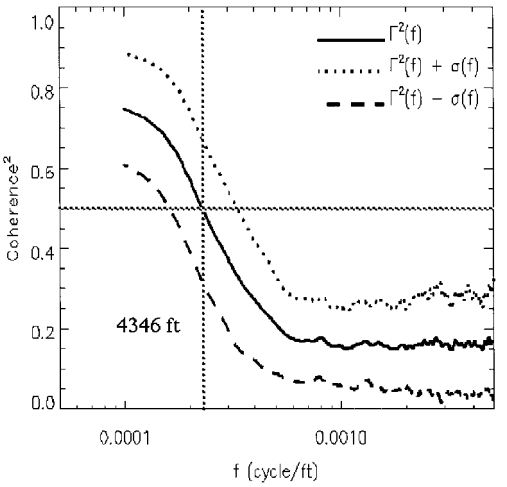

Fig. 21 Average coherence spectrum from 187 wind pairs measured 90 min apart.

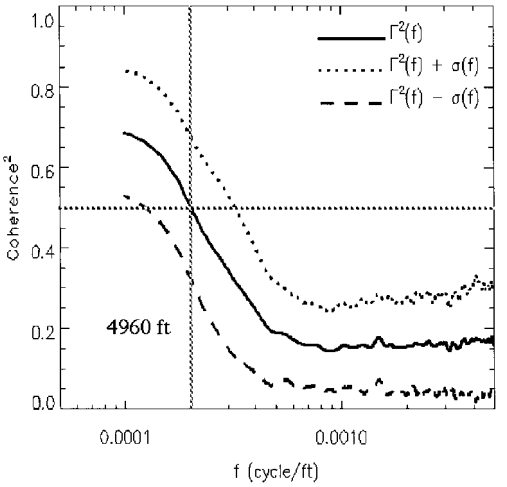

Fig. 22 Average coherence spectrum from 180 wind pairs measured 120 min apart.

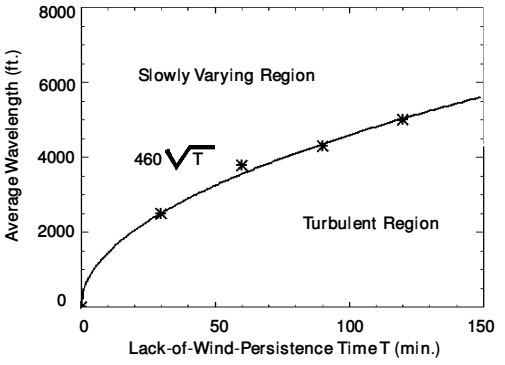

Fig. 23 Average wavelength boundary separating the slowly varying and turbulent components of winds as a function of elapsed time for winds measured at the Eastern and Western launch ranges during the months December through April.

This curve identifies the average boundary wavelength λ_B in the measured wind, as a function of time interval in minutes prior to launch. The boundary wavelength defines the average boundary between the slowly varying and the more rapidly varying (turbulent) portions of the wind. On the average for a time interval ΔT, wavelengths longer than λ_B are slowly varying, whereas wavelengths shorter than λ_B are rapidly varying.

Potential Uses

The boundary wavelengths in Eq. (14) are necessary to develop empirical gust loads analysis forcing functions[20] and to establish

loads caused by atmospheric turbulence.[21,22] Because the gust loads analysis accounts for the turbulent components of the winds statistically and the average boundary between the slowly varying and turbulent components of the winds can now be defined for the ER and WR ranges, there is the possibility of retaining in the day-of-launch loads analyses only those components of the winds that are slowly varying.[23] It is suggested that, to conservatively bracket the variation of this function, the values obtained with Eq. (14) be varied by an amount appropriate to the analysis being performed. A gust loads analysis in Refs. 20 and 21 is one such example.

Conclusions

This paper presented the results of work performed to determine the wavelength boundary between the slowly and rapidly varying components of the winds at the ER and WR of the United States. Methodology was developed and historical databases of winds were evaluated. Results include a simple function that relates the average boundary wavelength between slowly varying and turbulent components in measured winds to the time interval before launch. It was shown that longer vertical wavelengths of wind profiles are more slowly varying over time than shorter wavelengths.

As a result of this work, it is now possible to identify in measured wind profiles, as a function of time prior to launch, the slowly varying and the turbulent component of measured winds for two launch facilities. This information can be used to develop loads analyses using only the appropriate portion of the wind. It is believed that for several launch vehicles this will represent a reduction in loads and, hence, higher launch availability without a reduction in predicted reliability.

Acknowledgments

The authors are grateful to J. M. Womack of The Aerospace Corporation for his assistance in evaluating the statistical similarity of the coherence boundary wave numbers and for performing the rank sum test that established that the ER and WR boundary wavelengths for the more severe months can be treated as part of a single statistical family. Gratitude is also expressed to R. Walterscheid of The Aerospace Corporation for his helpful suggestions during several discussions regarding spectral analysis of wind data.

References

[1]Vail, J. R., "A Review of Space Vehicle Structural Design Problems During the Ascent Phase of Flight," TRW Corp., TRW Rept. 09425-6001-R000, Redondo Beach, CA, March 1968.

[2]Ryan, R. S., and King, A. W., "The Influential Aspects of Atmospheric Disturbances on Space Vehicle Design Using Statistical Approaches for Analysis," NASA TN D-4963, Jan. 1969.

[3]Smith, O. E., and Adelfang, S. I., "On the Relationship Between Wind Profiles and the STS Ascent Structural Loads," AIAA Paper 89-0709, Jan. 1989.

[4]Adelfang, S. I., "Analysis of Jimsphere Wind Profiles Viewed in the Flight Time Domain of a Saturn Vehicle," *Journal of Spacecraft and Rockets*, Vol. 7, No. 9, 1970, pp. 1146–1149.

[5]Smith, O. E., and Adelfang, S. I., "Wind Profile Models: Past, Present and Future for Aerospace Vehicle Ascent Design," AIAA Paper 98-1047, Jan. 1998.

[6]Luers, J., and Engler, N., "On Optimum Methods for Obtaining Wind Data from Balloon Sensors," *Journal of Applied Meteorology*, Vol. 6, Oct. 1967, pp. 816–823.

[7]Fleming, E. R., "Spacecraft and Launch Vehicle Loads," *Flight Vehicle Materials, Structures, and Dynamics*, Vol. 1, American Society of Mechanical Engineers, New York, 1991, Chap. 6.

[8]Kabe, A. M., "Design and Verification of Launch and Space Vehicle Structures," AIAA Paper 98-1718, April 1998.

[9]Macheske, V. M., Womack, J. M., and Binkley, J. F., "A Statistical Technique for Combining Launch Vehicle Atmospheric Flight Loads," AIAA Paper 93-0755, Jan. 1993.

[10]Womack, J. M., and Binkley, J. F., "A Statistical Technique for Combining Launch Vehicle Loads During Atmospheric Flight," The Aerospace Corp. TOR-0091(6530-06)-2, Los Angeles, Aug. 1992.

[11]Spiekermann, C. E., and Kabe, A. M., "Statistical Combination of Launch Vehicle Gust and Buffet Atmospheric Flight Loads," AIAA Paper 98-2010, April 1998.

[12]Binkley, J. F., Clark, J. B., and Spiekermann, C. E., "Improved Procedure for Combining Day-of-Launch Atmospheric Flight Loads," *Journal of Spacecraft and Rockets*, Vol. 37, No. 4, 2000, pp. 459–462.

[13]Meirovitch, L., *Elements of Vibration Analysis*, 2nd ed., McGraw–Hill, New York, 1986, pp. 238–240.

[14]Bendat, J. S., and Piersol, A. G., *Random Data Analysis and Measurement Procedures*, 2nd ed., Wiley-Interscience, New York, 1986, p. 409.

[15]Luers, J. K., and MacArthur, C. D., "Ultimate Wind Sensing Capabilities of the Jimsphere and Other Rising Balloon Systems," NASA CR-2048, June 1972.

[16]Johnson, D. L., and Vaughan, W. W., "Sequential High-Resolution Wind Profile Measurements," NASA TP 1354, Dec. 1978.

[17]Adelfang, S. I., Ashburn, E. V., and Court, A., "A Study of Jimsphere Wind Profiles as Related to Space Vehicle Design and Operations," NASA CR-1204, Nov. 1968.

[18]Wilfong, T., Smith, S., and Crosiar, C. L., "Characteristics of High-Wind Profiles Derived from Radar-Tracked Jimsphere and the Rose Processing Program," *Journal of Atmospheric and Oceanic Technology*, Vol. 14, No. 2, 1997, pp. 318–325.

[19]Hoel, P. G., Port, S. C., and Stone, C. J., *Introduction to Statistical Theory*, 1st ed., Houghton Mifflin Co., Boston, 1971, pp. 174–178.

[20]Sako, B. H., Kim, M. C., Kabe, A. M., and Yeung, W. K., "Derivation of Atmospheric Gust-Forcing Functions for Launch-Vehicle Loads Analysis," *Journal of Spacecraft and Rockets*, Vol. 37, No. 4, 2000, pp. 434–442.

[21]Kim, M. C., Kabe, A. M., and Lee, S. S., "Atmospheric Flight Gust Loads Analysis," *Journal of Spacecraft and Rockets*, Vol. 37, No. 4, 2000, pp. 446–452.

[22]Clark, J. B., Kim, M. C., and Kabe, A. M., "Statistical Analysis of Atmospheric Flight Gust Loads Analysis Data," *Journal of Spacecraft and Rockets*, Vol. 37, No. 4, 2000, pp. 443–445.

[23]Kabe, A. M., Spiekermann, C. E., Kim, M. C., and Lee, S. S., "Refined Day-of-Launch Atmospheric Flight Loads Analysis Approach," *Journal of Spacecraft and Rockets*, Vol. 37, No. 4, 2000, pp. 453–458.

A. M. Kabe
Guest Editor